Determining the Relative Contributions of Runoff and Coastal Processes to Flood Exposure across the Carolinas during Hurricane Florence

L. E. Grimley[1], A. Sebastian[1], T. Leijnse[2,3], D. Eilander[2,4], J. Ratcliff[1,5], and R. Luettich[1,5]

[1] Department of Earth, Marine and Environmental Sciences, University of North Carolina at Chapel Hill, Chapel Hill, NC, USA

[2] Institute for Environmental Studies (IVM), Vrije Universiteit Amsterdam, Amsterdam, the Netherlands.

[3] Department of Marine and Coastal Systems, Deltares, Delft, the Netherlands.

[4] Department of Inland and Water Systems, Deltares, Delft, the Netherlands.

[5] UNC Institute of Marine Sciences, Morehead City, NC, USA.

Corresponding author: Lauren Grimley (lauren.grimley@unc.edu)

Key Points:

- SFINCS reproduces observations of overland flooding from Hurricane Florence from 0-80 m+NAVD88 with a peak error of 0.09 m.
- The model predicts depths greater than 1.0 m at 96% of the locations where property-level records of insured damage occurred.
- Flood depths were 0.10 m higher at 23,251 buildings in the compound scenario than the maximum of either the coastal or runoff scenarios.

Abstract

Estimates of flood inundation from tropical cyclones (TCs) are needed to better understand how exposure varies inland and at the coast. While reduced-complexity flood inundation models have been previously shown to efficiently simulate the drivers of TC flooding across large regions, a lack of detailed validation studies of these models, which are being applied globally, has led to uncertainty about the quality of the predictions of inundation depth and extent and how this translates to exposure. In this study, we complete a comprehensive validation of a reduced-complexity hydrodynamic model (SFINCS) for simulating pluvial, fluvial, and coastal flooding. We hindcast Hurricane Florence (2018) flooding in North and South Carolina, USA using high-resolution meteorologic data and coastal water level output from an ocean recirculation model (ADCIRC). We compare modeled water levels to traditional validation datasets (e.g., water level gages, high-water marks) as well as property-level records of insured damage to draw conclusions about the model's performance. We demonstrate that SFINCS can accurately simulate coastal and runoff drivers of TC flooding at large scales with minimal computational requirements and limited calibration. We use the validated model to attribute flood extent and building exposure to the individual and compound flood drivers during Hurricane Florence. The results highlight the critical role runoff processes have in TC flood exposure and support the need for broader implementation of models that are capable of realistically representing the compound effects resulting from coastal and runoff processes.

Plain Language Summary

This study focuses on improving our understanding of flood risks caused by tropical cyclones (TCs). We use a flood inundation model to simulate flooding caused by Hurricane Florence (2018) in North and South Carolina, USA. The accuracy of the model is assessed by comparing modeled water levels to measurements taken in the field and records of property-level damage. We find that the model can accurately simulate TC flooding, including storm surge and rainfall, across large regions (e.g., watersheds) with minimal computational requirements and limited calibration. We also use the validated model to analyze flood extent and building exposure during Hurricane Florence, attributing them to storm surge or rainfall. The results emphasize the significant role that rainfall plays in TC flood exposure and the need for models capable of representing flooding from both coastal and runoff processes.

1 Introduction

Tropical Cyclones (TCs) generate widespread flooding that can lead to damages on the order of billions of US dollars (NCEI, 2023). TC flooding is influenced by multiple coastal and runoff drivers including mean sea level (MSL), surge, wind, rainfall, and streamflow (Gori et al., 2022; Lai et al., 2021). Evidence suggests that TC-related flood damages are increasing in response to changes in TC climatology and sea level rise (Meiler et al., 2022; Strauss et al., 2021), as well as development in coastal areas (Hallegatte et al., 2013; Pörtner et al., 2023; Hoeppe, 2016; Klotzbach et al., 2018; Merkens et al., 2016). For example, global annual costs associated with TCs tripled between 1990-2021 (Klotzbach et al., 2022) where the frequency of the most damaging storms is increasing at a higher rate than the moderately damaging storms (Grinsted et al., 2019). Yet, despite the rising costs associated with TCs, comprehensive risk assessments are lacking, as most previous studies neglect to assess the full extent of flood inundation from TCs, instead focusing on modeling individual flood drivers (e.g., storm surge or rainfall-runoff) at large scales (Bakhtyar et al., 2020; Colle et al., 2008; Dietrich et al., 2011; Ray et al., 2011; Torres et al., 2015), or compound flood drivers at smaller scales (e.g., an individual tributary (Gori, Lin, & Xi, 2020; Loveland et al., 2021) or urban area where substantial damages have occurred (Liu et al., 2022; Sebastian et al., 2021; Xu et al., 2022).

TC flooding can extend far beyond the coastline and landfall location as a result of rainfall-runoff and compound processes that drive flood inundation (Kunkel & Champion, 2019; Titley et al., 2021). However, many existing hydrodynamic models do not resolve the relevant physics (Santiago-Collazo et al., 2021) or are too computationally expensive to apply at large scales (Bates, 2021; Trigg et al., 2016; Wing et al., 2021). Increasingly, flood modelers are using reduced-physics solvers, subgrid options, and downscaling methods to overcome computational challenges associated with large scale (e.g., regional, continental, global) flood modeling (Leijnse et al., 2021; Neal et al., 2012, 2018; Sanders & Schubert, 2019). These methods are powerful because they balance computational speed and accuracy making them compatible with both deterministic and ensemble modeling approaches (Clare et al., 2022; Wing, Quinn, et al., 2020). However, in part due to lack of high-quality flood hazard observations in overland areas (Bates, 2023; Ward et al., 2015), validation of flood models is often limited, and has instead focused only on select gages in coastal areas (e.g., >20 m elevation) (Liu et al., 2022; Ye et al., 2021; Zhang et al., 2020) or riverine systems (Wing et al., 2017). As a result, there remains little information about model performance in overland areas, especially as it relates to pluvial processes. Given growing public interest in utilizing these approaches in both planning and forecasting applications, there is a need for an in-depth validation of their performance to better understand the uncertainty in the outputs (Jafarzadegan et al., 2023).

In this study, we address this gap by undertaking a transparent and detailed validation of a loosely coupled modeling approach using the numerical model Super-Fast INundation of CoastS (SFINCS) to hindcast pluvial, fluvial, and coastal flooding generated by Hurricane Florence (2018) in North (NC) and South Carolina (SC). SFINCS was built using the best available topobathymetric data and was forced with high-resolution meteorologic data and output from the ADvanced CIRCulation (ADCIRC) model at the coastal boundary. While previous studies of Hurricane Florence have focused on assessing model performance at a single site (Gori, Lin, & Smith, 2020) or by comparing model outputs to observational data typically below 20 m+NAVD88 (Nederhoff, Leijnse, et al., 2023; Ratcliff, 2022; Ye et al., 2021), we complete a comprehensive assessment of the full extent of flooding from inland (up to 200 m+NAVD88) to the coast across a large portion of the Carolinas. Modeled water levels were validated against point-level observations of flood inundation, including water level measurements at gages, high-water marks (HWMs), and property-level records of flood exposure. The validated model was then used to attribute building exposure to runoff (rainfall, discharge), coastal (wind, coastal water level) and compound flood drivers across the model domain. We demonstrate that our rapid modeling approach provides an accurate assessment of TC flooding both inland and at the coast making it useful for future planning and forecasting applications.

2 Background

The study area (77,655 sq.km.) encompasses portions of five USGS Hydrologic Unit Code (HUC) 6-digit watersheds spanning North and South Carolina including the Lower Pee Dee (LPD), Cape Fear (CF), Onslow Bay (OB), Neuse (N), and Pamlico (P) watersheds (Figure 1. This area experiences TC landfall on average every 5-8 years (NOAA & NHC, 2023). Notable historical hurricanes include Fran (1996), Floyd (1999), Matthew (2016), Florence (2018), and Dorian (2019). Of these, Hurricane Florence provides a uniquely large dataset against which to validate inundation models. Florence made landfall as a Category 1 storm near Wilmington, NC on September 14, 2018, and generated record-setting flooding across the two States (Hall &

Kossin, 2019; Kunkel & Champion, 2019). The highest land-based sustained winds averaged 79 kt (40.6 m/s), maximum storm surge heights across the Carolinas ranged between 0.9 and 3.4 m above MSL and rainfall totals ranged from 254 to 913 mm (Stewart & Berg, 2019). After landfall, Florence weakened and slowly moved farther inland across SC generating heavy precipitation over 2-4 days. Damages exceeded 2 billion USD (FEMA, 2020).

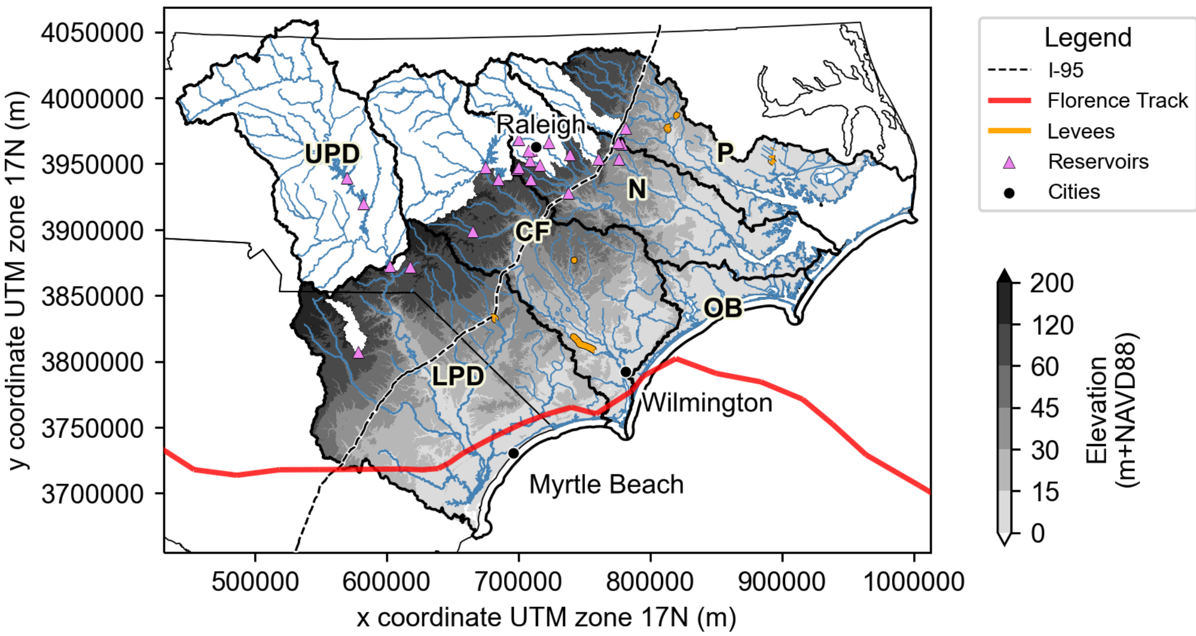

Figure 1. The study area includes five USGS HUC6 watersheds in North and South Carolina including the Lower Pee Dee (LPD), Cape Fear (CF), Neuse (N), Onslow Bay (OB), and Pamlico (P) which are outlined in black. The relative size of the Upper Pee Dee (UPD) basin which drains into the LPD is shown. Elevations in meters above the North American Vertical Datum of 1988 (NAVD88) are shown for the area included in the SFINCS model domain. The upstream boundary of the model was generally located downstream of large reservoirs (triangles) where river discharge is controlled. For context, the location of Wilmington and Raleigh, NC as well as Myrtle Beach, SC are shown in black dots. Hurricane Florence's storm track is a solid red line, Interstate 95 (I-95) is a dashed black line, and major levees are solid orange lines.

3 Methods

3.1 Hydrodynamic Model

We used the Super-Fast INundation of CoastS (SFINCS) hydrodynamic model to simulate multiple drivers of flooding at the river-coastal interface (van Ormondt et al., 2023). SFINCS is an open-source, open-access two-dimensional flood inundation model that uses a structured grid and accounts for spatially varying precipitation, infiltration, overland roughness, wind and atmospheric pressure (Leijnse et al., 2021). An advantage of SFINCS over other models is that it runs 'super-fast' because it computes overland flow using simplified equations of mass and momentum, uses an adaptive timestep, and supports OpenMP. SFINCS models can be created using an open-source Python package Hydro Model Tools (HydroMT) (Eilander, Boisgontier, et al., 2023) and the HydroMT-SFINCS plugin (Eilander, Leijnse, et al., 2022) making it easily replicated in new areas. These tools have successfully been used for model building in previous studies (Dullaart & van Manen, 2022; Eilander, Couasnon, Leijnse, et al., 2023).

SFINCS solves the Local Inertial Equations (i.e., SFINCS-LIE), based on the numerical solution used in the LISFLOOD-FP model (Bates et al., 2010) a wind drag term to account for wind stress. This is important especially for coastal applications where wind impact water levels. SFINCS also has the option to solve the Simplified Shallow Water Equations (i.e., SFINCS-SSWE) which includes an advection term, thus enabling it to predict super-critical flow conditions such as the propagation of locally generated surge and wave runup (Gaido et al., 2020). By default, SFINCS neglects the effect of atmospheric pressure gradients and the Coriolis force which is typically modeled in large-scale numerical ocean circulation models (Fringer et al., 2019). To account for offshore and ocean processes, SFINCS can be loosely coupled to ocean circulation models (e.g., the ADvanced CIRCulation model (ADCIRC) (Luettich & Westerink, 2004) or the Finite Volume Community Ocean Model (FVCOM) (Chen et al., 2003)) because it uses a 1D weakly reflective boundary condition. SFINCS generates coastal water levels accurately with reduced computation speeds when compared to other coastal hydrodynamic models (e.g., XBeach (Bertoncelj et al., 2021) and Delft3D FM (Röbke et al., 2021)).

To account for hydrologic processes, SFINCS can include a uniform constant infiltration value, spatially varying infiltration value, or apply the Soil Conservation Services (SCS) Curve Number (CN) Loss Model. The CN method calculates infiltration using the cumulative precipitation, antecedent moisture, and soil and land use type. Like most hydrodynamic models that use an explicit numerical scheme, SFINCS is restricted computationally by the spatial resolution of the structured grid but maintains speed and accuracy with an adaptive time step and subgrid method. The subgrid method is based on the principle that the bed level can vary substantially over short distances, but water levels vary over larger scales. Similar approaches have been tested and developed by Casulli (2009) and Volp et al. (2013). Coarse grid simulations which use cell averaged depth and velocities can overestimate the effects of friction leading to an underestimation of conveyance (this is traditionally corrected for through the calibration process). The SFINCS subgrid method accounts for bed level and roughness variations on a smaller scale than the native model grid (e.g., computation cell) in the computation of water fluxes by querying property tables. Results show that the subgrid feature in SFINCS enables increased computational speed without sacrificing model accuracy (Leijnse et al., 2020).

SFINCS has been shown to accurately capture total water levels from compound flooding in urban, coastal environments (Sebastian et al., 2021) and large watersheds (Eilander, Couasnon, et al., 2022), as well as tsunami offshore propagation and related flooding (Röbke et al., 2021). Because of its speed, SFINCS has been used to run large ensembles of storms (Eilander, Couasnon, Sperna Weiland, et al., 2023; Nederhoff, Leijnse, et al., 2023). It has also been previously applied to model flooding from Hurricane Florence on the U.S. Atlantic coast (Nederhoff, Leijnse, et al., 2023) however previous studies have predominantly focused on validating SFINCS output against water level gages and HWMs located below 20m +NAVD88. In this study, we evaluate SFINCS performance for simulating total water levels generated by Hurricane Florence, validating against water level observations that include elevations 80 m+NAVD88.

3.2 Model Setup

3.2.1 Model Inputs

The SFINCS model grid was generated with a spatial resolution of 200 m and active grid cells were designated using a modified shapefile of the NHD HUC6 boundaries as a mask (Figure 1). Cells outside of the mask were considered inactive. SFINCS cannot directly represent reservoir management, so the upstream boundary of the model was placed downstream of two large reservoirs in SC and five in NC (ranging between 150-200 m+NAVD88). Water level cells along the coastal boundary are on average at the -15 m+NAVD88 contour, specified using a modified shapefile of the National Hydrography Dataset (NHD) Area which delineates the extent of rivers and water bodies (see Figure S1 in Supplementary Materials). Where inter-basin flow might occur, outflow boundary cells – cells that allow water to drain from the model where it might otherwise unrealistically pool at the boundary – were designated (see Figure S2 in Supplementary Materials). Outflow can occur when extreme water levels flow between watershed boundaries, especially in low-gradient areas at the coast. The final model contains over 1.95 million active grid cells across the model domain which has an approximate area of 77,655 square kilometers (Figure 1).

Elevation and land cover data were interpolated to create a continuous raster at the resolution of the model grid and subgrid. Topographic and bathymetric DEMs are relative to the North American Vertical Datum of 1988 (NAVD88) including a 1.0 m USGS Coastal National Elevation Dataset (CoNED) for NC and SC, 1.0 m USGS National Elevation Dataset (NED) for SC, and a 0.3 m (1.0 ft) LiDAR-derived DEM for NC. Each raster was resampled to a 2.0 m spatial resolution using the Geospatial Data Abstraction Library (GDAL) and tiles of these 2.0 m DEMs were created using HydroMT so that they could be quickly read into python with the HydroMT-SFINCS plugin at an appropriate resolution before being interpolated to either the model grid or subgrid. After the model grid was generated, the 2.0 m DEMs were then used to populate subgrid derived tables for each grid cell. The subgrid file was generated at 5.0 m resolution as a pre-processing step such that property tables were built based on a specified refinement factor relative to the grid (here, 1/40th of the computational grid resolution). As the model grid and subgrid files are being written, HydroMT-SFINCS also generates elevation rasters at both resolutions which are used for downscaling the modeled water surface elevations.

River bathymetry was incorporated using over 100 interpolated triangular irregular networks (TINs) from HEC-RAS models maintained by North Carolina Department of Emergency Management (NCEM) (NCEM, 2020). For other rivers in NC, the maximum channel depth was extracted from the HEC-RAS cross-sections and interpolated to a 2.0 m raster corresponding to areas covered by the NHD Area polygon. For rivers that are not delineated by the NHD Area polygon, a constant channel width of 10.0 m was used to burn the maximum HEC-RAS cross-sectional depth as a rectangular channel into the DEM. Similar HEC-RAS data were not publicly accessible for water bodies in SC. Instead, 2.0 m was subtracted from the CoNED and NED datasets in the major channels and estuaries using the NHD Area polygon shapefile as a mask. A map identifying the locations and type of the channel bathymetry included in the model is shown in Supplementary Materials Figure S3.

Overland roughness coefficients were applied to the grid by assigning spatially varying Manning's coefficients to the land use/land cover (LULC) classes designated in the National

Land Cover Data (NLCD) 2019 Land Cover Product which classifies 16 land cover types at a 30-meter resolution for the nation (MRLC, 2022). Average values were used for the Manning's n friction coefficients that are within the range of plausible values (Arcement & Schneider, 1989; Chow et al., 1998; Savage et al., 2016) (see Supplementary Materials Table S1). In the NLCD LULC, there are locations where rivers might not be classified as open water because of their small size (less than 30m) or because they were assigned a developed land cover type due to bridge crossings. The raster of Manning's n values was updated for coastal water bodies using a modified shapefile of the NHD Area, for large rivers using the NHD Area, and for all other streams using the FRIS stream centerlines. Manning's n values were interpolated to a continuous raster at the subgrid resolution, and this was used to generate the subgrid property tables for each grid cell. CNs were specified at the grid resolution using the GCN250 dataset which has a spatial resolution of 250 m and was generated using global land cover and soils data (Jaafar et al., 2019). The CNs were used to compute spatial and temporally varying infiltration across the domain. Levees available from the National Levee Database (NLD) were incorporated into the model as weirs (weir coefficient of 0.6) (USACE, 2023). We assumed a crest of 1.0 m above the ground elevation.

3.2.2 Initial and Boundary Conditions

For the hindcast of Hurricane Florence, we used SFINCS-SSWE to simulate multi-mechanistic flooding over a 23-day simulation (September 7, 2018, 00:00 to September 30, 2018, 00:00). We also tested the sensitivity of the model results using SFINCS-LIE (i.e., no advection) and found that the recession (falling limb) of the hydrographs were better captured with advection. The difference in run time with and without advection was negligible.

Runoff processes were simulated by forcing the model using rainfall and streamflow observations. We applied NOAA's Multi-Radar Multi-Sensor (MRMS) Quantitative Precipitation Estimate (QPE) gridded rain-gage adjusted, radar-rainfall data directly to the model grid. We downloaded the MRMS data from the Iowa Environmental Mesonet archive (Iowa Environmental Mesonet, 2023). MRMS has a spatial resolution of 1.0 km and temporal resolution of 1-hour (the total precipitation for the entire simulation is shown in Figure S4 in the Supplementary Materials). At the upstream boundary of the model, we applied eight discharge time series from USGS gages (six reservoirs and two stream gages downstream of reservoirs) with a 15-minute temporal resolution (Supplementary Materials Figure S2). We do not include baseflow in our model.

Coastal processes were simulated by forcing the model using winds and coastal water levels (storm tide) modeled using a previously validated ADCIRC model for Hurricane Florence (Ratcliff, 2022). The ADCIRC model has a mean absolute error of 0.13 m and a root mean square error of 0.15 m when compared to peak water levels across NC. ADCIRC was forced with re-analyzed wind fields that are a modified version of the proprietary Ocean Weather Inc. (OWI) product that is shown to better replicate the strength and direction of winds during Hurricane Florence. We refer to this edited wind input as FLRA and it has a spatial resolution of 0.05-degree (~5.0 km) and a 15-minute temporal resolution (maximum FLRA wind speeds are shown in Figure S4 in the Supplementary Materials). FLRA wind data was applied to the SFINCS grid and wind drag coefficients from the Garratt linear drag law were used (Garratt, 1977). The wind drag coefficient varies linearly from 0.001-0.0025 between wind speeds of 0-28 m/s and then remains constant at 0.0025 for wind speeds greater than 28 m/s. The FLRA wind files were only available for the first 11 days of the simulation period from September 7, 2018 to September 18, 2018. After this, no wind was applied to the grid for the last 12 days of the simulation period. Storm tide was extracted at over 5,500 points in ADCIRC with an average grid spacing of 2.0 km in the estuary, sounds, and along the coastline and a 5.0 km spacing in the ocean. Points within 2.0 km distance from the water level boundary were interpolated to the SFINCS cell faces. ADCIRC time series with a 20-minute temporal resolution at 341 locations were interpolated to the cells along the coastal boundary in SFINCS (Supplementary Materials Figure S2). ADCIRC outputs are relative to MSL, and they were converted to NAVD88 using a correction-raster generated using NOAA’s Vertical Datum Transformation Tool (NOAA, 2022).

Initial soil moisture conditions were dry at the start of the simulation and the initial water level at the coast was set to 0.25 m+NAVD88. The model uses a 24-hour startup period allowing the coastal water level to stabilize, filling the bays and estuaries with water. Discharge, coastal water level, precipitation, and wind inputs are applied to the model starting seven days prior to Hurricane Florence landfall (September 14, 2018) allowing river channels to fill and the antecedent soil moisture conditions to be set.

We conducted sensitivity analysis as a form of calibration of the model where we compared performance metrics for varying grid resolution (e.g., 100 vs 200 m), Manning's n (e.g., average vs. high values), and presence/absence of channels. This information is reported in Tables S2 and S3 in the Supplementary Materials. We did not do any quality control of the input datasets or detailed calibration of model parameters because we are looking at a single event and do not want to overfit the model. Water levels across the entire domain are output every hour. The model computational time was 1.2 hours using a machine with 48 CPUs and an average timestep of six seconds.

4 Results

4.1 Model Validation

We performed a detailed validation of the model across the study area comparing modeled timeseries at 89 water level gages, peak water levels at 512 USGS HWMs, and flood depths to property-level records of insured damage.

4.1.1 Water Levels

We compared the modeled water levels at 89 water level gages (76 USGS, five NOAA, seven USGS Rapid Deployment, one NCEM) across the entire simulation. We show results for all stations that had at least 50 measurements during the simulation period, even if they had gaps or missed the peak. The timing of peak water levels from coastal and runoff processes varied by HUC6 basins. In some cases, the hydrographs in major rivers and estuaries did not recede for many days. Calculating the stats for the flood hydrograph, which often had double peaks in the coastal zone, at each gage would have required uniquely specifying the time window at each gage. We calculated the stats using all observational data that was available at each gage for the entire 23-day simulation including normal flow conditions.

At each gage, we calculated the Peak Error (PE), Bias (also known as the Mean Error), Root-Mean-Square-Error (RMSE), and the Coefficient of Determination (R-squared). The PE is a useful indicator of peak flood extent which is important for estimating exposure and damage. We calculated the Bias to quantify whether the model tends to under or overpredict the observed water levels across the simulation. We used the RMSE to quantify the absolute deviations between modeled and observed water levels (i.e., the spread) noting that the RMSE highlights large errors. Lastly, we calculated the R-squared which is a commonly applied measure in hydrology to measure the 'goodness-of-fit' between model simulations and observations (Krause et al., 2005). R-squared estimates the combined dispersion to the individual dispersion of the modeled and observed data where a value of zero indicates poor model performance and a higher value is associated with good model performance. The R-squared metric is not a perfect measure and does not indicate whether there is a systematic bias meaning it can be low for an accurate model or high for an inaccurate model. However, these metrics are widely used for estimating the predictive ability of the model to replicate measured water levels (Jackson et al., 2019).

We calculated these statistics at each gage (see Table S4 in the Supplementary Materials) which are shown in

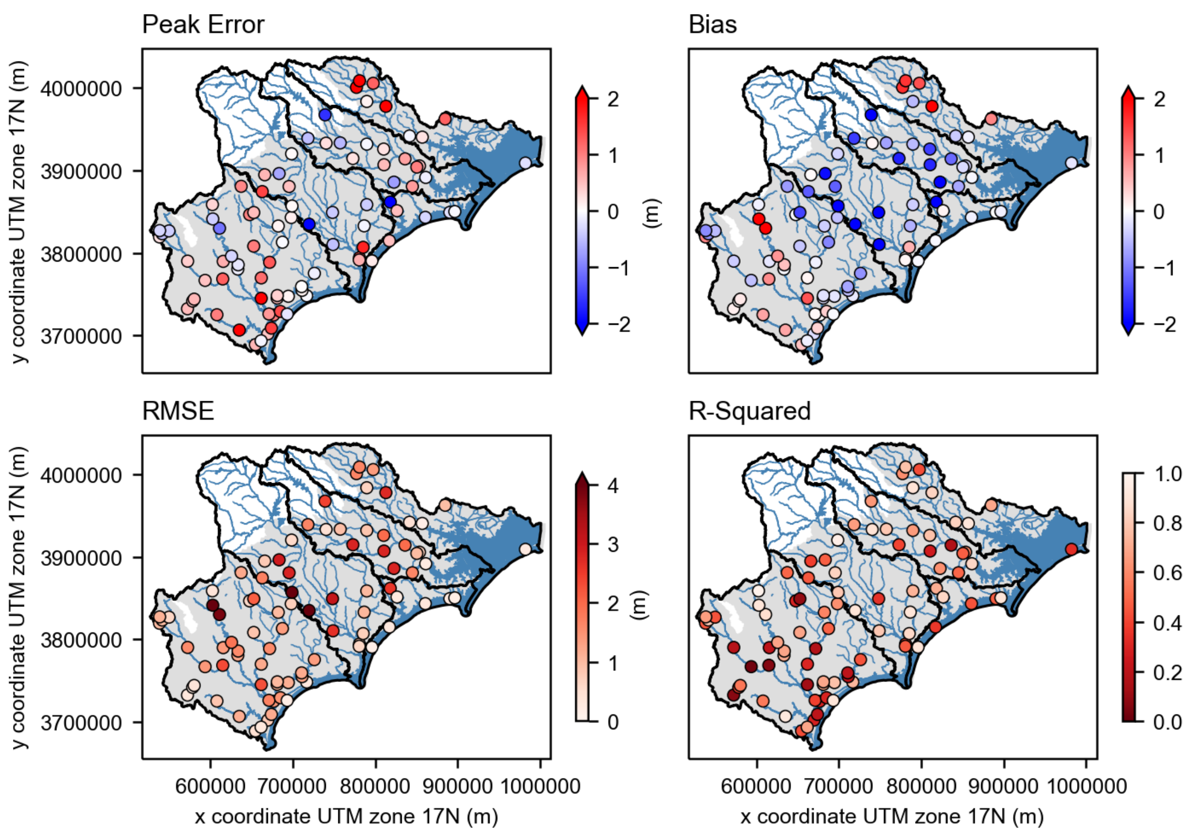

Figure 2. At water level gages, the model has an average peak error of 0.33 m and tends to overpredict the peak, especially in the Lower Pee Dee watershed. The model has an average bias of -0.29 m, an RMSE of 1.17 m and an R-squared of 0.56. We calculated the average statistic for each HUC6 basin which is provided in Table 1. The model tends to overpredict water levels in the Pamlico and Lower Pee Dee watersheds where bathymetry data was limited. In the Neuse, Cape Fear, and Onslow Bay basins where higher detailed information on channel

bathymetry was available, the peak error tends to be smaller, but the mean error indicates the model tends to underpredict water levels across the model domain. The higher R-squared values in NC watersheds indicate the model's predictive skill is slightly better in this area of the domain where channel bathymetry is specified than in the Lower Pee Dee.

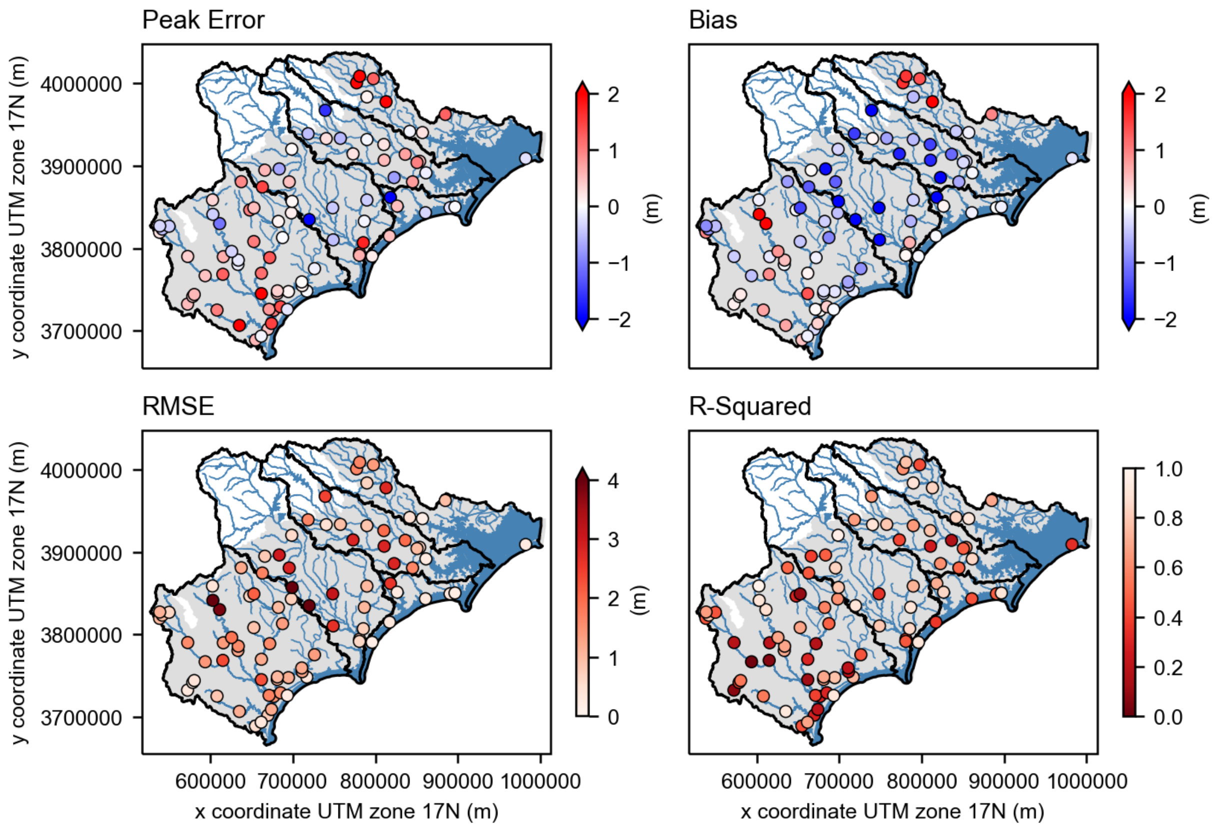

Figure 2. Peak Error (m), Bias (m), Root-Mean-Square-Error (RMSE) (m), and Coefficient of Determination (R-squared) statistics were calculated for Hurricane Florence at 89 gages.

Table 1. Modeled water levels were compared to gage observations using statistics of the Peak Error, Bias, Root-Mean-Square-Error (RMSE), and Coefficient of Determination (R-squared) which were calculated across the 23-day simulation. These metrics were averaged across the gages for each HUC6 watershed and for the entire domain.

HUC6 Watershed	Peak Error (m)	Bias (m)	RMSE (m)	R-squared
Cape Fear	0.15	-1.24	2.07	0.66
Lower Pee Dee	0.43	0.06	1.24	0.48
Neuse	0.04	-1.08	1.60	0.59
Onslow Bay	-0.21	-0.32	0.56	0.65
Pamlico	1.07	0.77	1.11	0.70
Domain	0.33	-0.29	1.35	0.56

4.1.2 Peak Water Levels

To further assess how well the model predicts flooding during Hurricane Florence, we compared the peak modeled water levels against USGS observed HWMs. We downloaded HWMs from the USGS Flood Event Viewer (USGS, 2023b) and filtered them to select those that had a quality of 'Fair: +/−0.12 m', 'Good: +/−0.03 m', or 'Excellent: +/−0.015 m'. The subset of HWMs included 512 locations across the domain including elevations up to 80 m+NAVD88 (358 locations in NC and 154 locations in SC). When compared against all HWMs, the model has an average bias of 0.05 m and RMSE of 0.93 m. The model tends to underpredict in NC but overpredict in SC as shown in Figure 3. This pattern is also reflected in the comparison to water level time series at gages.

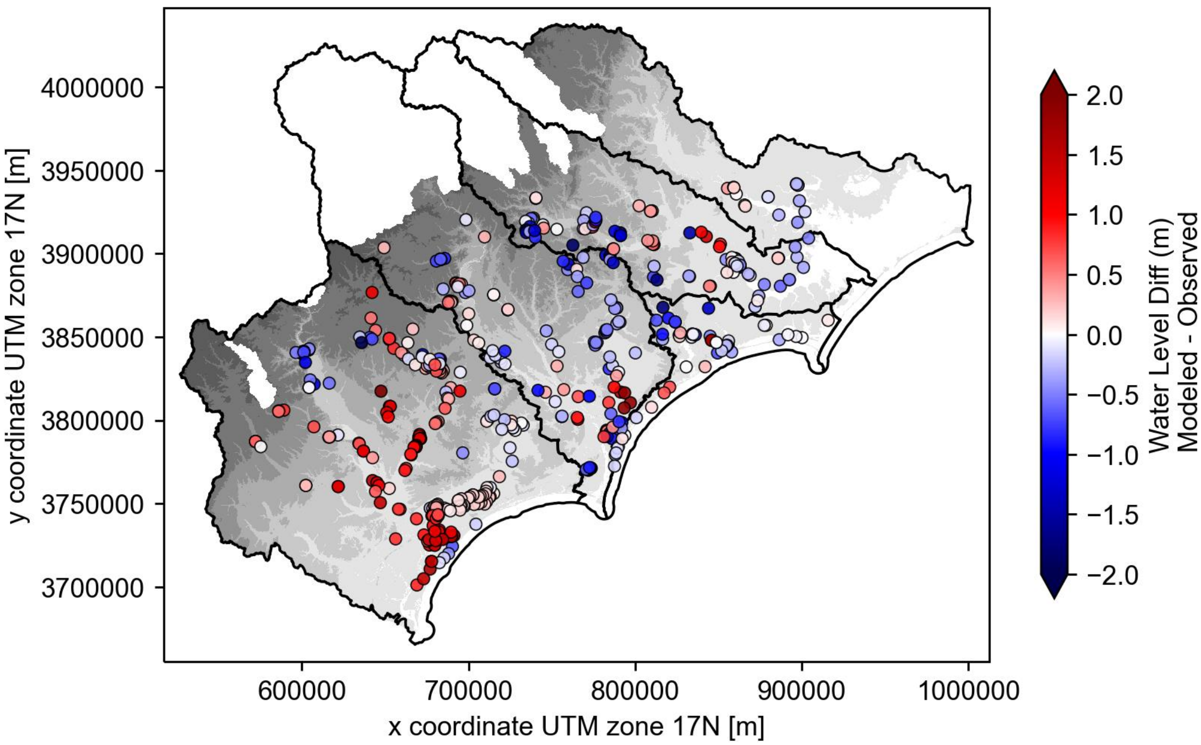

Figure 3. Modeled peak water levels for Hurricane Florence were compared to observations at 512 USGS high-water marks (HWMs) with a quality of 'fair' or better. The bias (m) is shown at each location. The model tends to overpredict (positive values in red) in SC with more underprediction (negative values in blue) in NC.

To enable easy comparison with other flood modeling studies of Hurricane Florence, we compare the modeled and observed water levels at HWM locations across the entire domain, the coastal zone, and a subset of the inland (Figure . The model consistently overpredicts peak water levels in the Lower Pee Dee watershed but underpredicts across the HUC6 watersheds in NC. A histogram of the model error (m) for the coastal and inland zone is shown in Figure S4 in the Supplementary Materials and the average bias and RMSE for each HUC6 are listed in Table S4.

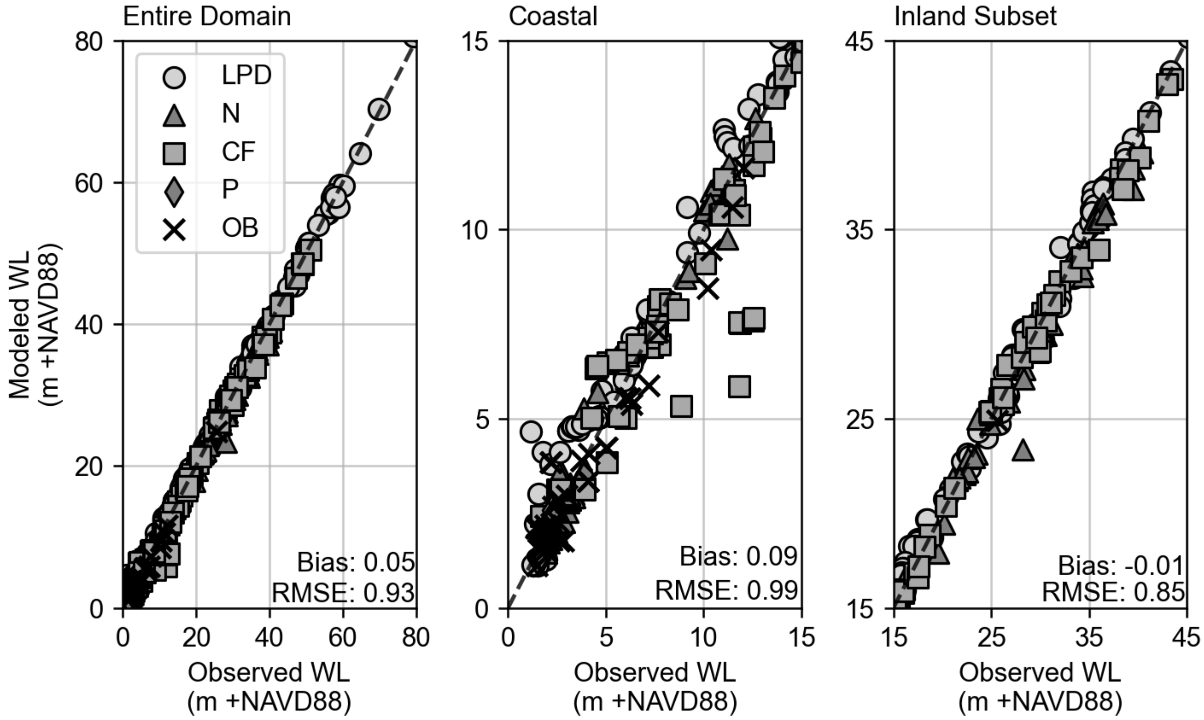

Figure 4. Observed and modeled peak water levels were compared at 512 USGS High Water Mark (HWM) locations across the five HUC6 watersheds: Lower Pee Dee (LPD), Neuse (N), Cape Fear (CF), Pamlico (P), and Onslow Bay (OB). The three QQ-plots (1:1 plots) show this comparison for all the HWM locations (left), coastal zone <= 15 m+NAVD88 (middle), and a subset of the inland areas between 15 and 45 m+NAVD88 (right). Note: the scale of the axis changes for each subplot and the model bias and RMSE for the data shown is listed in the bottom right corner.

4.1.3 Property-level Building Exposure

While flood hazard outputs are often used to estimate infrastructure exposure, reports of building damage have not been widely used to assess flood hazard model performance. Due to privacy concerns, this data is typically only available aggregated to administrative units (e.g., census tracts, zip codes, counties), making it difficult to use for model validation (Bates, 2023; Wing, Pinter, et al., 2020). For example, the NOAA Storm Events Database provides storm and damage data for flash floods by county, whereas floods and tropical weather are reported by the National Weather Service (NWS) Forecast zone (NWS, 2023). As part of a study of Hurricane Florence and its impacts commissioned by the NC Legislature (NC Policy Collaboratory, 2021), we obtained property-level records of National Flood Insurance Program (NFIP) policies and claims data from FEMA Region IV for the State of NC. NFIP claims and policies were geocoded and joined to a dataset of building footprints (North Carolina Floodplain Mapping Program, 2022). We then selected policies and claims that were dated between September 6 and 30, 2018 (as in Thomson et al. (2023)). This resulted in 11,073 buildings with a NFIP claim and 11,739 buildings associated with a NFIP policy but no claim. These 22,812 buildings were 1.5% of the total buildings within the NC portion of the model domain (n=1,488,229).

We used this property-level dataset to generate a contingency matrix to assess how well the model predicts building exposure (i.e., where reported damage or no damage serves as a proxy). The contingency matrix includes true positives (X), false positives (Y), true negatives (Z), and false negatives (W) calculated using a flood depth threshold. The number of events is equal to the total number of locations that reported damage (i.e., E=X+Y) and the total number of cases is equal to the events and the total number of locations that reported no damage (i.e., C=E+Z+W). When the model predicts flooding above a specified depth threshold at a structure that is associated with a claim, it was considered a true positive. Conversely, a false positive occurs when the model does not predict flooding at a structure where a claim was filed. A building might also be associated with a policy but not a claim which we assumed means the household did not experience flooding. A false negative occurs when the model predicts flooding at a building that had a policy but was not associated with a claim. A true negative occurs when the model did not predict flooding at a building that had a policy but not claim.

To calculate the contingency matrix, we used bilinear interpolation to downscale the modeled peak water level at the grid resolution (i.e., 200 m) to the subgrid resolution (i.e., 5 m) to generate a flood depth raster. Water depths below 0.05 m were excluded. The water depth at each structure is extracted from this modeled inundation raster at the building centroid. We used depth thresholds of 0.05, 0.25, 0.5, and 1.0 m to classify buildings as flooded or not flooded. Using the information from the contingency matrix, we calculated forecast verification metrics. These metrics were first employed to indicate the value of flood warning (Schaefer, 1990) and more recently for modeled flood extent to other model output (Bates et al., 2021) or remotely sensed flood extents (Courty et al., 2017; Eilander, Couasnon, Leijnse, et al., 2023). We calculated the following metrics for each flood threshold which are reported in Table 3:

- Accuracy is the fraction of the modeled flooded and non-flooded locations that were correctly predicted where Accuracy = (X+Z) / C.
- Bias measures the ratio of the frequency of modeled flooded locations to the frequency of observed damaged locations where Bias = ((X+Z) / E) - 1. A tendency to underpredict is BIAS < 0 while a tendency to overpredict is BIAS > 0.
- Probability of Detection (POD), also known as hit rate, is the fraction of modeled flooded locations (e.g., true positives) that were correctly predicted where POD = X / E. This score does not penalize for false negatives.
- False Alarm Ratio (FAR) is the fraction of modeled flooded locations that were not correctly predicted (e.g., no damage reported) where FAR = X / (X+Z).
- Success Ratio (SR) is the fraction of the modeled flooded locations that were observed where SR = X / (X+Z).
- The Critical Success Index (CSI) measures the ratio of the modeled flooded locations to the observed where CSI = X / (E+Z). The CSI is sensitive to the number of true positives and penalizes both the false positives and false negatives.

The highest accuracy occurs using the 1.0 m depth where the model correctly predicts 84% of the cases (n=22,812) of damage or and no damage. At this depth threshold the model has the lowest FAR of 4% but the largest bias of -0.28. Across all depth thresholds, the model correctly predicts flooding at 69% (POD) of the total locations that reported damage (n=11,073) which matches the tendency of the model to underpredict the number of flooded locations (bias <0). The fraction of the modeled flooded locations that were correctly observed ranges between 83% and 96% (SR). The best CSI score of 0.68 is obtained when using the depth threshold of 1.0 m but the difference between depth thresholds is minimal.

Table 2. We used the contingency matrix of true positives, false positives, true negatives, and false negatives computed using the 22,812 property-level records of insured damage from Hurricane Florence for NC buildings to calculate forecast verification metrics using multiple depth thresholds.

Forecast Verification Metric	Perfect Score	Flood Depth Threshold (m)			
		0.05	0.25	0.50	1.0
Accuracy	1	0.78	0.80	0.82	0.84
Bias	0	-0.17	-0.21	-0.24	-0.28
Probability of Detection (POD)	1	0.69	0.69	0.69	0.69
False Alarm Rate (FAR)	0	0.17	0.13	0.09	0.04

Success Ratio (SR)	1	0.83	0.87	0.91	0.96
Critical Success Index (CSI)	1	0.61	0.63	0.65	0.68

4.2 Flood Driver Attribution

Using the validated SFINCS model, we simulated multiple scenarios applying various combinations of the individual forcings for Hurricane Florence including river discharge (Q), precipitation (P), coastal water level (C), and wind (W). Using the outputs, we explored how the different forcings alter flood patterns across the study area. Pluvial and fluvial flooding is difficult to disentangle when modeling rainfall-runoff across large watersheds for extreme rainfall events. Therefore, we grouped pluvial and fluvial flooding as runoff processes. The runoff scenario included Q and P forcings with a constant coastal water level (C=0 m+NAVD88) and no wind. The coastal scenario included C and W forcings with no rainfall or discharge inputs. Our analysis focused on comparing the compound scenario to the coastal and runoff.

We computed the difference in peak water level between the compound scenario (C+W+Q+P) and the largest depth from the coastal (C+W) and runoff (Q+P) model scenarios as shown in Figure 6. Areas that experienced the greatest increase in water level due to the combination of all drivers were primarily in the coastal transition zone (e.g., below 15 m). In Figure 6, we show the dominant drivers (i.e., coastal and runoff). Darker colors indicate areas where the compound scenario amplified total water levels by at least 0.05 m. The combination of all forcings exacerbates peak water levels especially in areas adjacent to the floodplain and major estuaries.

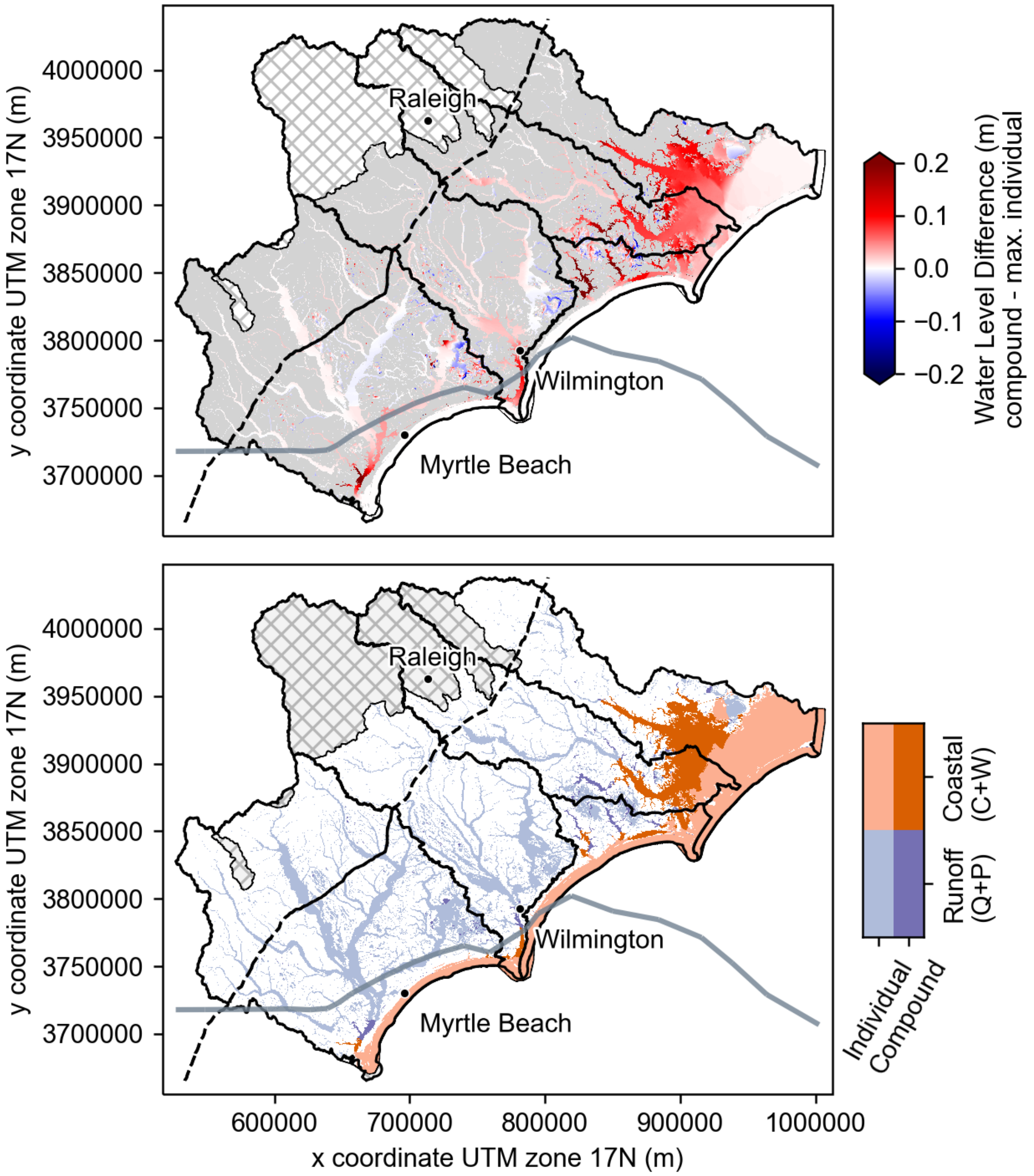

Figure 5. The top panel shows the difference in peak water level between the compound scenario which includes the coastal water level (C), wind (W), discharge (Q), and precipitation (P) forcings and the largest depth from the coastal (C+W) and runoff (Q+P) model scenarios. The bottom panel shows the dominant drivers (i.e., coastal and runoff) which are darker for areas where the compound scenario increased total water levels by at least 0.05 m.

We used the downscaled flood depth maps for the compound, coastal, and runoff scenarios to calculate peak flood extents and estimate building exposure. To calculate the flooded area, we summed the area of all the cells that had flood depths greater than 0.05 m. The flooded area is greater for the runoff than the coastal scenario, however, the compound scenario inundated the largest area (Table 4). We used the National Structure Inventory (NSI) maintained by the USACE to estimate building exposure in SC and a more recently updated dataset of building footprints available from NCEM for NC. Within the model domain, there are an estimated 1,488,229 buildings in NC and 428,051 in SC. We extracted the flood depth at each building centroid for each of the three scenarios. The mean depth of water at buildings for all three scenarios is reported in Table 4. The number of structures exposed to flooding for the compound scenario is greater than the sum of the runoff and coastal scenarios. Compound flooding increased water levels by 0.10 m (+/- 0.06 m) at 23,251 buildings (28.7% of total exposed) considering locations where depth differences were greater than 0.05 m between the compound scenario and the maximum of any individual driver. In the compound scenario, an additional 4,347 buildings (5.4 % of total exposed) were exposed to flooding that were not exposed to flooding in the individual runoff or coastal scenarios. At these locations, the average depth was 0.14 m (+/- 0.15 m) (see Figure S7).

Table 3. The flood extent and mean depth at buildings for the coastal, runoff, and compound scenarios were determined using flood maps at the subgrid resolution.

Model Scenario	Total Area Flooded (sq.km.)	No. of Buildings w/ Flood Depth > 0.05 m	Mean Flood Depth at Buildings (m)
Coastal (C+W)	11,717 (15.1% of domain)	32,563 (1.7% of total)	0.62 (+/- 0.51)
Runoff (Q+P)	23,809 (30.7% of domain)	47,055 (2.5% of total)	0.90 (+/- 0.95)
Compound (C+W+Q+P)	25,604 (33.0% of domain)	81,121 (4.2% of total)	0.80 (+/- 0.82)

We show descriptive statistics for the depth at buildings for each watershed in Figure 7. We calculated the fraction of buildings exposed to runoff and coastal processes for each HUC6 basin. For each building exposed to flooding from coastal processes in the Pamlico, Neuse, and Onslow Bay there were 13, 2, and 5 buildings exposed to runoff processes, respectively (i.e., building exposure primarily to runoff processes). Conversely, for each building exposed to flooding from runoff processes in the Cape Fear and Lower Pee Dee there were 54 and 163 exposed to flooding from coastal processes, respectively (i.e., building exposure primarily to coastal processes).

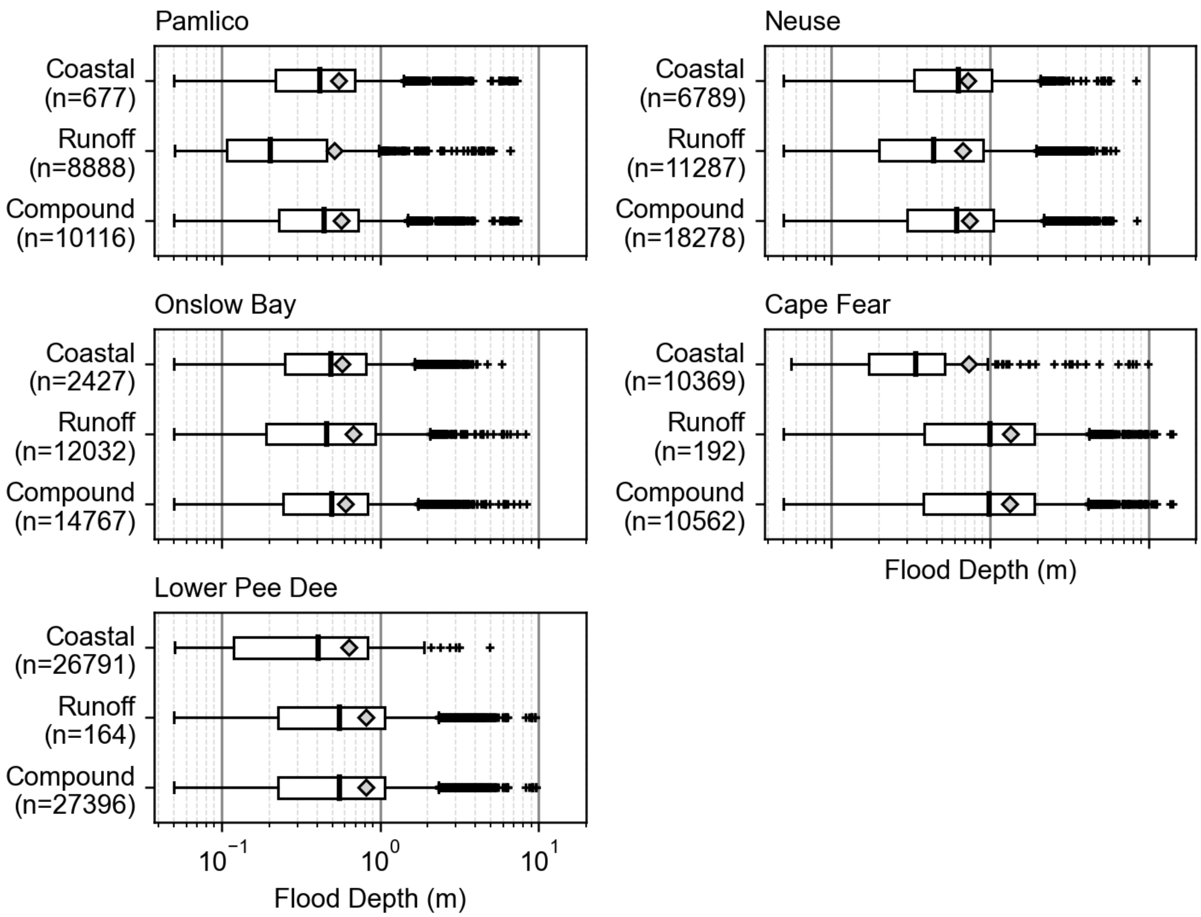

Figure 6. Flood depths at buildings for the runoff (Q+P), coastal (C+W) and compound (C+W+Q+P) scenarios grouped by HUC6 basin. Water depth is logged on the x-axis. The median is indicated by thick black line and the mean is noted by a grey diamond. The number of buildings (n) is listed below the scenario name.

5 Discussion

5.1 Simulating total water levels inland and at the coast

We hindcasted flooding from Hurricane Florence across NC and SC using the hydrodynamic model SFINCS. We developed the model using the best available data but did not perform extensive calibration beyond a few sensitivity tests of the Manning's values and grid resolution. Two-dimensional hydrodynamic models have the advantage of simulating the bi-directional propagation of water, but their performance is restricted by the accuracy of the elevation data used (Bates, 2021). Having well-represented channels and water bodies is crucial for improving compound flood hazard estimates because the interaction between streamflow, rainfall, and coastal water levels and coastal tides is heavily dictated by the shape of the channel (Cooper, 2002; Harrison et al., 2022; Leuven et al., 2018; Yankovsky et al., 2012). However, national scale digital elevation models do not include channels and there is a lack of readily accessible information on channel characteristics to incorporate into the model (Neal et al., 2021). While there is bathymetry available in the major coastal water bodies across the southeast Atlantic coast (e.g., CoNED and CUDEM), this data does not extend far upstream into the estuaries, and it is not clear where the information is "real" measurements or an artifact of geoprocessing (see, e.g., hydro-flattening in USGS (2023a)). When available, we took advantage of local datasets with channel information, enabling us to represent channels of widths less than <30m. However, we assumed a rectangular channel with a constant depth which may overestimate the cross-sectional area of flow which has been previously shown to be important for estimating conveyance and floodplain exchange (Dey et al., 2019; Slater, 2016).

We addressed this for the major rivers in NC by manually including bathymetric information in our DEM obtained by extracting river channel characteristics from over 100 HEC-RAS 1D models. This took a substantial amount of time because the data was not easy easily accessible from the model files. The model peak error is 0.09 m (n=601 including bias at 512 HWMs, PE at 89 gages). The model peak error is smaller in the HUC6 watersheds where channel bathymetry was represented in the model for all inland rivers (Supplementary Materials Table S2 and S3). Specifically, the peak error of the model across the Pamlico, Neuse, Cape Fear and Onslow Bay watersheds was -0.19 m (n=324). Conversely, the peak error of the model was 0.43 m (n=277) in the Lower Pee Dee watershed where we assumed a "burned in" channel with depths of 2.0 m for major river bodies that were identified in the NHD Area polygon. However, the model has a negative bias when considering the errors across the 23-day simulation particularly for inland rivers in NC where channels were included. During low or normal flow conditions, the in-channel water levels are low compared to observations skewing the overall bias to negative. This might be occurring in the model because of a lack of baseflow or the simplified rectangular channels over or underestimating channel conveyance. The model bias and peak error is smaller at the coast where improved bathymetry is available in national datasets (e.g., CUDEM, CoNED). We expect that incorporating channel bathymetry for all streams would improve channel routing and conveyance in the model.

In addition to channel bathymetry, there are other several other potential sources of uncertainty. First, we did not explicitly account for streamflow obstructions, such as small weirs/dams or bridge piers, in the DEM or Manning's roughness. These structures can alter the propagation of streamflow and possibly slow down channel flow which could impact the shape of the hydrograph (Bates, 2021). There are ongoing efforts to create databases of infrastructure (Nienhuis et al., 2022) and corrected DEMs that can be incorporate into models (Schumann & Bates, 2018; Woodrow et al., 2016). We do not account for subsurface infrastructure (e.g., sewers) but we expect their influence on the extent of pluvial flooding to be small as they were likely completely inundated during this extreme event. Second, there is some uncertainty in the total volume of rainfall-runoff the model generates given the simplicity of the infiltration scheme used as well as the coarseness of the input soil information. Though the SCS Curve Number Method is widely used in hydrologic modeling, other infiltration schemes (such as Green-Ampt) can harness additional soil information for improved runoff estimation. Third, we did not investigate the uncertainty in the model forcings but used the best available products. The meteorological data (e.g., wind, rainfall) can contribute to model errors when hindcasting hydrodynamic processes resulting from TCs (Rahman et al., 2022; Ratcliff, 2022). For example, the temporal and spatial resolution of the data applied can impact the timing and volume of runoff computed by hydrologic models (Quintero et al., 2022). We used gage-corrected rainfall and wind products that have the finest spatial and temporal resolution available. However, the wind data was limited to the first 11 days of the 23-day simulation which could impact the performance of the model, especially at the coast.

In general, the model performance is in line with other studies that use 2D reduced-physics hydrodynamic models to simulate flooding (Saksena et al., 2020; Sebastian et al., 2021) and we see similar model performance for other storms (see S3 in the Supplementary Materials for validation results of Hurricane Matthew). We conclude that the model shows skill for simulating compound flooding at large spatial scales when compared to HWMs and water level gages making it useful tool for understanding how the different drivers contribute to changes in flood hazard and exposure.

5.2 Using property-level records of insured damage to further assess flood models

We also used property-level records of insured damage in NC to better evaluate model performance in areas with limited gage data or HWMs (e.g., outside of floodplains). We calculated an average CSI of 0.64 which indicates adequate model performance. The CSI used alone can mask large differences between modeled and observations (Bates et al., 2021; Eilander, Couasnon, Leijnse, et al., 2023) so we report the additional scores to provide context. The fraction of the modeled flooded and non-flooded locations that are correctly predicted (Accuracy) is 84% using a depth threshold of 1.0 m. Across all depth thresholds, the model correctly predicts 69% of the damage locations (POD). However, the model tends to underpredict flooded locations with an average bias score of -0.23. When considering only the damaged locations (e.g., claim filed), the model correctly predicts flooding at 96% (SR) of these structures using a depth threshold of 1.0 m. These scores are similar to other studies that compare modeled flood extent to satellite images of flooding (Courty et al., 2017; Sosa et al., 2020; Wing et al., 2017, 2021). The skill scores indicate that the model is generally predicting flooding in areas where it likely occurred (a claim filed) across the entire domain (**Error! Reference source not found.**). A depth threshold of 1.0 m results in the best forecast scores overall, but this is likely because using smaller depth thresholds may lead to a conservative (high) estimate of the number of flooded buildings.

Despite the promise of the above statistics, it is important to point out that our analysis does not consider first floor elevation because there is large uncertainty in the estimates since the data was only collected in 2010 for buildings inside the SFHA and buildings outside of the floodplain are assigned a single first floor elevation. We also did not average the water depths across each building footprint and only select a single depth at the centroid. When comparing this dataset to OpenFEMA which reports NFIP policies and claims at the census block group scale, we found that the total number of claims matched but the number of policies was significantly underrepresented in the property-level dataset (approximately 30% of the total reported in (FEMA, 2023). It is unclear how this introduces error into the skill metrics. The Accuracy, FAR, and CSI scores could improve or worsen depending on if the model predicts flooding at these locations where we are missing policy information.

5.3 Delineating the drivers of total water levels and exposure

We used the SFINCS model to simulate Hurricane Florence flooding with different forcings applied to investigate how the flood extent and building exposure changes when considering the various drivers (e.g., coastal, runoff, and compound). The compound scenario results in a peak water level that is +/- 0.15 m compared to the model results with either coastal or runoff alone. These differences primarily occur in the coastal zone (e.g., below 15 m+NAVD88). Figure 6 demonstrates that the water levels in the coastal zone of the Pamlico and Neuse basins were dominated by coastal processes, especially wind (Figure S8 in the Supplementary Materials). Conversely, in the Lower Pee Dee the total water levels were primarily controlled by runoff processes. While we combined the pluvial and fluvial components into the runoff scenario, the watershed that experienced the largest contribution from streamflow was the Lower Pee Dee since another large HUC6 watershed (Upper Pee Dee) drains into it at the upstream boundary (Figure 1). This is evident when attributing the dominant forcing to water levels as shown in Figure S4 in the Supplementary Materials. In the Cape Fear and Onslow Bay watersheds we see that both coastal and runoff processes were important for determining water levels along the estuaries and floodplains.

Using the peak flood depth maps at the subgrid resolution, we calculated the total area that was flooded at depths greater than 0.05 m across the three scenarios (Table 4). The coastal, runoff, and compound processes inundate 15.1%, 30.7%, and 33.0% of the model domain, respectively, and the corresponding mean flood depths at the exposed buildings were 0.62 m, 0.90 m, and 0.80 m. In general, the flood depths modeled at exposed buildings tended to be greater for the runoff scenario compared to the coastal scenario, especially at locations in SC. Using the model and building footprint datasets, we estimated that more than 81,121 buildings were exposed to flooding from Hurricane Florence (i.e., 64,570 in NC (4.3% of total NC buildings in domain) and 16,551 in SC (3.7% of total SC building in domain)). In SC, the number that experienced actual flood damage could be smaller given that the model tends to overpredict the peak and many homes are elevated above ground level. We find that water levels and flood depths at buildings are exacerbated in the compound scenario, particularly in the coastal zone, highlighting the importance of process-based models for predicting compound flooding. These results highlight that the drivers of TC flood exposure for Hurricane Florence varies over a large area (e.g., five HUC6 watersheds) and the combination of runoff and coastal processes is important for a comprehensive assessment.

6 Conclusions

Flood exposure from TCs can extend far beyond coastal areas as extreme rainfall can generate significant pluvial and fluvial flooding that can exacerbate flooding in coastal communities and further inland (Gori, Lin, & Xi, 2020; Pricope et al., 2022; Sebastian et al., 2021). In this study, we complete an in-depth validation of the reduced-complexity hydrodynamic model (SFINCS) loosely coupled to an ocean circulation model (ADCIRC). We chose SFINCS because it represents processes important for simulating TC flooding (e.g., wind, sea level, rainfall, streamflow) and is fast, scalable, and easily applied in new areas using open-source tools it. We loosely couple SFINCS to ADCIRC but it has also been previously coupled to Delft3D see e.g., (Nederhoff, Crosby, et al., 2023). We hindcast runoff and coastal processes from Hurricane Florence to predict water levels across five HUC6 watersheds in the Carolinas. We perform a detailed validation of the model comparing against observed water levels (89 water level gages, 512 HWM locations) and property-level records of insured damage (n=22,812). Our study provides new insights into model performance in inland areas outside of the coastal zone (i.e., areas >20m +NAVD88). The model shows skill in simulating runoff and coastal processes with a bias of 0.05 m and RMSE of 0.93 m compared to observed HWMs ranging up to 80 m+NAVD88. In areas where channels are not included in the terrain (e.g., Lower Pee Dee watershed in SC), the model tends to overpredict water levels. The model correctly predicts flooding at 96% of the damage and non-damage locations using a depth threshold of 1.0 m. However, we also discuss that translating modeled inundation to estimates of building exposure is highly uncertain and can vary depending on the chosen depth threshold and the characteristics of the structure (e.g., first floor elevation).

Community flood resilience can be facilitated by a better understanding of the flood drivers which are both controlled by the watershed and stream network characteristics as well as the temporal and spatial resolution of the storm (e.g., landfall location, wind speeds). We also completed a comprehensive assessment of the contribution of runoff and coastal drivers to flood extent across the model domain and building exposure in NC. We modeled three scenarios including coastal (wind, sea level), runoff (rainfall, streamflow) and compound. The compound scenario resulted in an additional 1,503 buildings (1.9% of total buildings exposed) exposed to flooding than the total of the individual runoff and coastal drivers, suggesting that the compound processes may increase water levels nonlinearly. However, the locations where compound flooding exacerbates total water levels may also shift depending on the initial conditions of the system (e.g., mean sea level, streamflow) and the spatial variations in the meteorology (wind, rainfall) associated with a given TC, and as a result, is difficult to extrapolate observations of the compound processes observed during Hurricane Florence to other TCs which may impact the Carolinas. Future work should examine additional events to identify where compound flood hazards are possible.

As TCs continue to pose a threat to many coastlines, it is important to accurately predict both the coastal and runoff processes to get a complete picture of risk. This study demonstrates that SFINCS is a suitable tool for TC flood hazard and exposure assessment because it can simulate multiple mechanisms of flooding (e.g., wind, sea level, rainfall, streamflow) with minimal computational requirements and limited calibration. The speed and flexibility of SFINCS makes it easy to quickly generate flood-related information across large spatial scales. Yet, similar to previous studies which employ large-scale flood models (see e.g., (Neal et al., 2021; Saksena et al., 2020)) the accurate representation of channel bathymetry is important to model performance, but data availability continues to be a challenge (Bates, 2023; Dey et al., 2019).

The model can be further improved by testing the sensitivity of the results to higher spatial resolution dataset for soil infiltration (e.g., through finer resolution of soil data with the Soil Survey Geographic Database (SSURGO)), the explicit inclusion of levees (e.g., using levee data from the USACE National Levee Database (NLD)), large reservoirs (e.g., using levees/weirs in combination with culvert structure with specified rating curve), and bridge piers (e.g., through increased Manning's n values). The uncertainty in the meteorologic forcing inputs could also be further explored by using an ensemble of wind and rainfall inputs (e.g., Stage IV radar-rainfall, ERA5 reanalysis) (Grimley et al., 2020). Lastly, this study could be expanded to include additional types of meteorologic events, tropical and non-tropical, to better delineate the areas that experience compound flooding.

Acknowledgments

We thank K. Fitzmaurice at the Center on Financial Risk in Environmental Systems (CoFiRES) at UNC Chapel Hill for helping to geocode the property-level data. We would also like to acknowledge K. Nederhoff and R. de Goede at Deltares for fruitful discussion and software support. This research was supported by the North Carolina General Assembly and the North Carolina Policy Collaboratory through Session Law 2019-224. L.E.G., A.S., and R.L. were supported by the National Science Foundation (GCR-2021086) as a part of the Dynamics of Extreme Events, People, and Places (DEEPP) project at the University of North Carolina at Chapel Hill. L.E.G. was also supported by a graduate research fellowship with the North Carolina Water Resources Research Institute (WRRI) and North Carolina Sea Grant. The authors are grateful to the North Carolina Department of Emergency Management and FEMA Region IV for access to data. The authors declare no conflicts of interest relevant to this study.

References

Arcement, G. J., & Schneider, V. R. Guide for Selecting Manning's Roughness Coefficients for Natural Channels and Flood Plains, USGS § (1989).

Bakhtyar, R., Maitaria, K., Velissariou, P., Trimble, B., Mashriqui, H., Moghimi, S., et al. (2020). A New 1D/2D Coupled Modeling Approach for a Riverine-Estuarine System Under Storm Events: Application to Delaware River Basin. *Journal of Geophysical Research: Oceans*, *125*(9). https://doi.org/10.1029/2019JC015822

Bates, P. D. (2021). Flood Inundation Prediction. *Annual Review of Fluid Mechanics*, *54*(1), 287–315. https://doi.org/10.1146/annurev-fluid-030121-113138

Bates, P. D. (2023). Fundamental limits to flood inundation modelling. *Nature Water*, *1*(7), 566–567. https://doi.org/10.1038/s44221-023-00106-4

Bates, P. D., Horritt, M. S., & Fewtrell, T. J. (2010). A simple inertial formulation of the shallow water equations for efficient two-dimensional flood inundation modelling. *Journal of Hydrology*, *387*(1–2), 33–45. https://doi.org/10.1016/j.jhydrol.2010.03.027

Bates, P. D., Quinn, N., Sampson, C., Smith, A., Wing, O., Sosa, J., et al. (2021). Combined Modeling of US Fluvial, Pluvial, and Coastal Flood Hazard Under Current and Future Climates. *Water Resources Research*, *57*(2), 1–29. https://doi.org/10.1029/2020WR028673

Bertoncelj, V., Leijnse, T., Roelvink, F., Pearson, S., Bricker, J., Tissier, M., & van Dongeren, A. (2021). Efficient and accurate modeling of wave-driven flooding on coral reef-lined coasts: Case Study of Majuro Atoll, Republic of the Marshall Islands. In *EGU General Assembly*. https://doi.org/doi.org/10.5194/egusphere-egu21-5418

Casulli, V. (2009). A high-resolution wetting and drying algorithm for free-surface hydrodynamics. *International Journal for Numerical Methods in Fluids*, *60*(4), 391–408. https://doi.org/10.1002/fld.1896

Chen, C., Liu, H., & Beardsley, R. C. (2003). An Unstructured Grid, Finite-Volume, Three-Dimensional, Primitive Equations Ocean Model: Application to Coastal Ocean and Estuaries. *Journal of Atmospheric and Oceanic Technology*, *20*(1), 159–186. https://doi.org/10.1175/1520-0426(2003)020<0159:AUGFVT>2.0.CO;2

Chow, V. Te, Maidment, D. R., & Mays, L. W. (1998). *Applied Hydrology*. (B. J. Clark & J. Morriss, Eds.) (Applied Hy). McGraw-Hill Book Company. Retrieved from http://ponce.sdsu.edu/Applied_Hydrology_Chow_1988.pdf

Clare, M. C. A., Leijnse, T. W. B., McCall, R. T., Diermanse, F. L. M., Cotter, C. J., & Piggott, M. D. (2022). Multilevel multifidelity Monte Carlo methods for assessing uncertainty in coastal flooding. *Natural Hazards and Earth System Sciences*, *22*(8), 2491–2515. https://doi.org/10.5194/nhess-22-2491-2022

Colle, B. A., Buonaiuto, F., Bowman, M. J., Wilson, R. E., Flood, R., Hunter, R., et al. (2008). New York City's Vulnerability to Coastal Flooding. *Bulletin of the American Meteorological Society*, *89*(6), 829–842. https://doi.org/10.1175/2007BAMS2401.1

Cooper, J. A. G. (2002). The role of extreme floods in estuary-coastal behaviour: Contrasts between river- and tide-dominated microtidal estuaries. *Sedimentary Geology*, *150*(1–2), 123–137. https://doi.org/10.1016/S0037-0738(01)00271-8

Courty, L. G., Pedrozo-Acuña, A., & Bates, P. D. (2017). Itzï (version 17.1): an open-source, distributed GIS model for dynamic flood simulation. *Geoscientific Model Development*, *10*(4), 1835–1847. https://doi.org/10.5194/gmd-10-1835-2017

Dey, S., Saksena, S., & Merwade, V. (2019). Assessing the effect of different bathymetric models on hydraulic simulation of rivers in data sparse regions. *Journal of Hydrology*, *575*(July 2018), 838–851. https://doi.org/10.1016/j.jhydrol.2019.05.085

Dietrich, J. C., Westerink, J. J., Kennedy, A. B., Smith, J. M., Jensen, R. E., Zijlema, M., et al. (2011). Hurricane Gustav (2008) Waves and Storm Surge: Hindcast, Synoptic Analysis, and Validation in Southern Louisiana. *Monthly Weather Review*, *139*(8), 2488–2522. https://doi.org/10.1175/2011MWR3611.1

Dullaart, J., & van Manen, S. (2022). *An Assessment of the Impacts of Climate Change on Coastal Inundation on Bonaire*. Amsterdam.

Eilander, D., Couasnon, A., Leijnse, T., Ikeuchi, H., Yamazaki, D., Muis, S., et al. (2022). A globally-applicable framework for compound flood hazard modeling. *EGUsphere*, *2022*(April), 1–40.

Eilander, D., Leijnse, T., & Winsemius, H. C. (2022). hydroMT-sfincs (v0.2.1). Zenodo. https://doi.org/10.5281/zenodo.6244556

Eilander, D., Couasnon, A., Leijnse, T., Ikeuchi, H., Yamazaki, D., Muis, S., et al. (2023). A globally applicable framework for compound flood hazard modeling. *Natural Hazards and Earth System Sciences*, *23*(2), 823–846. https://doi.org/10.5194/nhess-23-823-2023

Eilander, D., Boisgontier, H., Bouaziz, L. J. E., Buitink, J., Couasnon, A., Dalmijn, B., et al. (2023). HydroMT: Automated and reproducible model building and analysis. *Journal of Open Source Software*, *8*(83), 4897. https://doi.org/10.21105/joss.04897

Eilander, D., Couasnon, A., Sperna Weiland, F. C., Ligtvoet, W., Bouwman, A., Winsemius, H. C., & Ward, P. J. (2023). Modeling compound flood risk and risk reduction using a globally applicable framework: a pilot in the Sofala province of Mozambique. *Natural Hazards and Earth System Sciences*, *23*(6), 2251–2272. https://doi.org/10.5194/nhess-23-2251-2023

FEMA. (2023). OpenFEMA Dataset: FIMA NFIP Redacted Policies - v2. Retrieved August 1, 2023, from https://www.fema.gov/api/open/v2/FimaNfipPolicies

Fringer, O. B., Dawson, C. N., He, R., Ralston, D. K., & Zhang, Y. J. (2019). The future of coastal and estuarine modeling: Findings from a workshop. *Ocean Modelling*, *143*(September), 101458. https://doi.org/10.1016/j.ocemod.2019.101458

Gaido, C., Nederhoff, K., Reguero, B. G., Storlazzi, C. D., Leijnse, T., Dongeren, A. van, et al. (2020). From regional flood risk analysis to local: comparing coastal flooding in Miami Beach with XBeach and SFINCS. In *AGUFM*. https://doi.org/2020AGUFMNH0380012G

Garratt, J. R. (1977). Review of Drag Coefficients over Oceans and Continents. *Monthly Weather Review*, *105*(7), 915–929. https://doi.org/10.1175/1520-0493(1977)105<0915:RODCOO>2.0.CO;2

Gori, A., Lin, N., & Smith, J. (2020). Assessing Compound Flooding From Landfalling Tropical Cyclones on the North Carolina Coast. *Water Resources Research*, *56*(4). https://doi.org/10.1029/2019WR026788

Gori, A., Lin, N., & Xi, D. (2020). Tropical Cyclone Compound Flood Hazard Assessment: From Investigating Drivers to Quantifying Extreme Water Levels. *Earth's Future*, *8*(12). https://doi.org/10.1029/2020EF001660

Gori, A., Lin, N., Xi, D., & Emanuel, K. (2022). Tropical cyclone climatology change greatly exacerbates US joint rainfall-surge hazard. *Nature Portfolio*. https://doi.org/10.1038/s41558-021-01272-7

Grimley, L. E., Quintero, F., & Krajewski, W. F. (2020). Streamflow Predictions in a Small Urban–Rural Watershed: The Effects of Radar Rainfall Resolution and Urban Rainfall–Runoff Dynamics. *Atmosphere*, *11*(8), 774. https://doi.org/10.3390/atmos11080774

Grinsted, A., Ditlevsen, P., & Christensen, J. H. (2019). Normalized US hurricane damage estimates using area of total destruction, 1900−2018. *Proceedings of the National Academy of Sciences*, *116*(48), 23942–23946. https://doi.org/10.1073/pnas.1912277116

Hall, T. M., & Kossin, J. P. (2019). Hurricane stalling along the North American coast and implications for rainfall. *Npj Climate and Atmospheric Science*, *2*(1), 17. https://doi.org/10.1038/s41612-019-0074-8

Hallegatte, S., Green, C., Nicholls, R. J., & Corfee-Morlot, J. (2013). Future flood losses in major coastal cities. *Nature Climate Change*, *3*(9), 802–806. https://doi.org/10.1038/nclimate1979

Harrison, L. M., Coulthard, T. J., Robins, P. E., & Lewis, M. J. (2022). Sensitivity of Estuaries to Compound Flooding. *Estuaries and Coasts*, *45*(5), 1250–1269. https://doi.org/10.1007/s12237-021-00996-1

Hoeppe, P. (2016). Trends in weather related disasters – Consequences for insurers and society. *Weather and Climate Extremes*, *11*, 70–79. https://doi.org/10.1016/j.wace.2015.10.002

Iowa Environmental Mesonet. (2023). Iowa Environmental Mesonet (IEM) Archive.

Jaafar, H. H., Ahmad, F. A., & El Beyrouthy, N. (2019). GCN250, new global gridded curve numbers for hydrologic modeling and design. *Scientific Data*, *6*(1), 145. https://doi.org/10.1038/s41597-019-0155-x

Jackson, E. K., Roberts, W., Nelsen, B., Williams, G. P., Nelson, E. J., & Ames, D. P. (2019). Introductory overview: Error metrics for hydrologic modelling – A review of common practices and an open source library to facilitate use and adoption. *Environmental Modelling & Software*, *119*(May), 32–48. https://doi.org/10.1016/j.envsoft.2019.05.001

Jafarzadegan, K., Moradkhani, H., Pappenberger, F., Moftakhari, H., Bates, P., Abbaszadeh, P., et al. (2023). Recent Advances and New Frontiers in Riverine and Coastal Flood Modeling. *Reviews of Geophysics*, *61*(2). https://doi.org/10.1029/2022RG000788

Klotzbach, P. J., Bowen, S. G., Pielke, R., & Bell, M. (2018). Continental U.S. Hurricane Landfall Frequency and Associated Damage: Observations and Future Risks. *Bulletin of the American Meteorological Society*, *99*(7), 1359–1376. https://doi.org/10.1175/BAMS-D-17-0184.1

Klotzbach, P. J., Wood, K. M., Schreck, C. J., Bowen, S. G., Patricola, C. M., & Bell, M. M. (2022). Trends in Global Tropical Cyclone Activity: 1990–2021. *Geophysical Research Letters*, *49*(6). https://doi.org/10.1029/2021GL095774

Krause, P., Boyle, D. P., & Bäse, F. (2005). Comparison of different efficiency criteria for hydrological model assessment. *Advances in Geosciences*, *5*, 89–97. https://doi.org/10.5194/adgeo-5-89-2005

Kunkel, K. E., & Champion, S. M. (2019). An Assessment of Rainfall from Hurricanes Harvey and Florence Relative to Other Extremely Wet Storms in the United States. *Geophysical Research Letters*, *46*(22), 13500–13506. https://doi.org/10.1029/2019GL085034

Lai, Y., Li, J., Gu, X., Liu, C., & Chen, Y. D. (2021). Global compound floods from precipitation and storm surge: Hazards and the roles of cyclones. *Journal of Climate*, *34*(20), 1–55. https://doi.org/10.1175/JCLI-D-21-0050.1

Leijnse, T., Nederhoff, K., Dongeren, A. van, McCall, R., & van Ormondt, M. (2020). Improving Computational Efficiency of Compound Flooding Simulations: the SFINCS Model with Subgrid Features.

Leijnse, T., van Ormondt, M., Nederhoff, K., & van Dongeren, A. (2021). Modeling compound flooding in coastal systems using a computationally efficient reduced-physics solver: Including fluvial, pluvial, tidal, wind- and wave-driven processes. *Coastal Engineering*, *163*(December 2019), 103796. https://doi.org/10.1016/j.coastaleng.2020.103796

Leuven, J. R. F. W., van Maanen, B., Lexmond, B. R., van der Hoek, B. V., Spruijt, M. J., & Kleinhans, M. G. (2018). Dimensions of fluvial-tidal meanders: Are they disproportionally large? *Geology*, *46*(10), 923–926. https://doi.org/10.1130/G45144.1

Liu, Q., Xu, H., & Wang, J. (2022). Assessing tropical cyclone compound flood risk using hydrodynamic modelling: a case study in Haikou City, China. *Natural Hazards and Earth System Sciences*, *22*(2), 665–675. https://doi.org/10.5194/nhess-22-665-2022

Loveland, M., Kiaghadi, A., Dawson, C. N., Rifai, H. S., Misra, S., Mosser, H., & Parola, A. (2021). Developing a Modeling Framework to Simulate Compound Flooding: When Storm Surge Interacts With Riverine Flow. *Frontiers in Climate*, *2*(February). https://doi.org/10.3389/fclim.2020.609610

Luettich, R. A., & Westerink, J. (2004). *Formulation and Numerical Implementation of the 2D / 3D ADCIRC Finite Element Model Version 44.XX*.

Meiler, S., Vogt, T., Bloemendaal, N., Ciullo, A., Lee, C.-Y., Camargo, S. J., et al. (2022). Intercomparison of regional loss estimates from global synthetic tropical cyclone models. *Nature Communications*, *13*(1), 6156. https://doi.org/10.1038/s41467-022-33918-1

Merkens, J.-L., Reimann, L., Hinkel, J., & Vafeidis, A. T. (2016). Gridded population projections for the coastal zone under the Shared Socioeconomic Pathways. *Global and Planetary Change*, *145*, 57–66. https://doi.org/10.1016/j.gloplacha.2016.08.009

MRLC. (2022). Multi-Resolution Land Characteristics Consortium.

NC Policy Collaboratory. (2021). *Collaboratory Flood Resiliency Study*. Retrieved from https://collaboratory.unc.edu/wp-content/uploads/sites/476/2021/06/flood-resiliency-report.pdf

NCEI. (2023). NOAA National Centers for Environmental Information (NCEI) U.S. Billion-Dollar Weather and Climate Disasters. https://doi.org/10.25921/stkw-7w73

NCEM. (2020). North Carolina Flood Risk Information System (FRIS). Retrieved November 11, 2020, from fris.nc.gov

Neal, J., Schumann, G., & Bates, P. D. (2012). A subgrid channel model for simulating river hydraulics and floodplain inundation over large and data sparse areas. *Water Resources Research*, *48*(11), 1–16. https://doi.org/10.1029/2012WR012514

Neal, J., Dunne, T., Sampson, C., Smith, A., & Bates, P. D. (2018). Optimisation of the two-dimensional hydraulic model LISFOOD-FP for CPU architecture. *Environmental Modelling & Software*, *107*(May), 148–157. https://doi.org/10.1016/j.envsoft.2018.05.011

Neal, J., Hawker, L., Savage, J., Durand, M., Bates, P., & Sampson, C. (2021). Estimating River Channel Bathymetry in Large Scale Flood Inundation Models. *Water Resources Research*, *57*(5), 1–22. https://doi.org/10.1029/2020WR028301

Nederhoff, K., Crosby, S., VanArendonk, N., Grossman, E., Tehranirad, B., Leijnse, T., et al. (2023). Dynamic modeling of coastal compound flooding hazards due to tides, extratropical storms, waves, and sea-level rise: a case study in the Salish Sea, Washington (USA). *EarthArXiv*. https://doi.org/10.31223/X5S945

Nederhoff, K., Leijnse, T., Parker, K., Thomas, J., O’Neill, A., van Ormondt, M., et al. (2023). Tropical or extratropical cyclones: what drives the compound flood hazard, impact, and risk for the United States Southeast Atlantic coast? *EarthArXiv*. Retrieved from https://doi.org/10.31223/X56H26

Nienhuis, J. H., Cox, J. R., O’Dell, J., Edmonds, D. A., & Scussolini, P. (2022). A global open-source database of flood-protection levees on river deltas (openDELvE). *Natural Hazards and Earth System Sciences*, *22*(12), 4087–4101. https://doi.org/10.5194/nhess-22-4087-2022

NOAA. (2022). Vertical Datum Transformation v4.3. NOAA.

NOAA, & NHC. (2023). Tropical Cyclone Climatology. Retrieved October 23, 2023, from https://www.nhc.noaa.gov/climo/

North Carolina Floodplain Mapping Program. (2022). North Carolina Flood Risk Information System.

NWS. (2023). NOAA Storm Events Database. Retrieved October 22, 2023, from https://www.ncdc.noaa.gov/stormevents/

van Ormondt, M., Leijnse, T., Nederhoff, K., de Goede, R., & van Dongeren, A. (2023). SFINCS: Super-Fast INundation of CoastS model (2.0.2 Blockhaus Release Q2 2023). Zenodo. https://doi.org/10.5281/zenodo.8038565

Pörtner, H.-O., Roberts, D. C., Poloczanska, E. S., Mintenbeck, K., Tignor, M., Alegría, A., et al. (2023). IPCC, 2022: Summary for Policymakers. In *Climate Change 2022 – Impacts, Adaptation and Vulnerability* (pp. 3–34). Cambridge University Press. https://doi.org/10.1017/9781009325844.001

Pricope, N. G., Hidalgo, C., Pippin, J. S., & Evans, J. M. (2022). Shifting landscapes of risk: Quantifying pluvial flood vulnerability beyond the regulated floodplain. *Journal of Environmental Management*, *304*(December 2021), 114221. https://doi.org/10.1016/j.jenvman.2021.114221

Quintero, F., Villarini, G., Prein, A. F., Krajewski, W. F., & Zhang, W. (2022). On the role of atmospheric simulations horizontal grid spacing for flood modeling. *Climate Dynamics*, *59*(11–12), 3167–3174. https://doi.org/10.1007/s00382-022-06233-0

Rahman, M. A., Zhang, Y., Lu, L., Moghimi, S., Hu, K., & Abdolali, A. (2022). Relative accuracy of HWRF reanalysis and a parametric wind model during the landfall of Hurricane Florence and the impacts on storm surge simulations. *Natural Hazards*, (0123456789). https://doi.org/10.1007/s11069-022-05702-3

Ratcliff, J. (2022). *Analysis of Wind and Storm Surge of Hurricane Florence*. https://doi.org/10.17615/zrvv-mq88

Ray, T., Stepinski, E., Sebastian, A., & Bedient, P. B. (2011). Dynamic Modeling of Storm Surge and Inland Flooding in a Texas Coastal Floodplain. *Journal of Hydraulic Engineering*, *137*(10), 1103–1110. https://doi.org/10.1061/(asce)hy.1943-7900.0000398

Röbke, B. R., Leijnse, T., Winter, G., van Ormondt, M., van Nieuwkoop, J., & de Graaff, R. (2021). Rapid Assessment of Tsunami Offshore Propagation and Inundation with D-FLOW Flexible Mesh and SFINCS for the 2011 Tōhoku Tsunami in Japan. *Journal of Marine Science and Engineering*, *9*(5), 453. https://doi.org/10.3390/jmse9050453

Saksena, S., Dey, S., Merwade, V., & Singhofen, P. J. (2020). A Computationally Efficient and Physically Based Approach for Urban Flood Modeling Using a Flexible Spatiotemporal Structure. *Water Resources Research*, *56*(1), 1–22. https://doi.org/10.1029/2019WR025769

Sanders, B. F., & Schubert, J. E. (2019). PRIMo: Parallel raster inundation model. *Advances in Water Resources*, *126*(October 2018), 79–95. https://doi.org/10.1016/j.advwatres.2019.02.007

Savage, J. T. S., Pianosi, F., Bates, P., Freer, J., & Wagener, T. (2016). Quantifying the importance of spatial resolution and other factors through global sensitivity analysis of a flood inundation model. *Water Resources Research*, *52*(11), 9146–9163. https://doi.org/10.1002/2015WR018198

Schaefer, J. T. (1990). The Critical Success Index as an Indicator of Warning Skill. *Weather and Forecasting*.

Schumann, G. J.-P., & Bates, P. D. (2018). The Need for a High-Accuracy, Open-Access Global DEM. *Frontiers in Earth Science*, *6*(December), 1–5. https://doi.org/10.3389/feart.2018.00225

Sebastian, A., Bader, D. J., Nederhoff, C. M., Leijnse, T. W. B., Bricker, J. D., & Aarninkhof, S. G. J. (2021). Hindcast of pluvial, fluvial, and coastal flood damage in Houston, Texas during Hurricane Harvey (2017) using SFINCS. *Natural Hazards*, (2017). https://doi.org/10.1007/s11069-021-04922-3

Slater, L. J. (2016). To what extent have changes in channel capacity contributed to flood hazard trends in England and Wales? *Earth Surface Processes and Landforms*, *41*(8), 1115–1128. https://doi.org/10.1002/esp.3927

Sosa, J., Sampson, C., Smith, A., Neal, J., & Bates, P. (2020). A toolbox to quickly prepare flood inundation models for LISFLOOD-FP simulations. *Environmental Modelling & Software*, *123*(October 2019), 104561. https://doi.org/10.1016/j.envsoft.2019.104561

Stewart, S. R., & Berg, R. (2019). *Hurricane Florence*.

Strauss, B. H., Orton, P. M., Bittermann, K., Buchanan, M. K., Gilford, D. M., Kopp, R. E., et al. (2021). Economic damages from Hurricane Sandy attributable to sea level rise caused by anthropogenic climate change. *Nature Communications*, *12*(1), 2720. https://doi.org/10.1038/s41467-021-22838-1

Thomson, H., Zeff, H. B., Kleiman, R., Sebastian, A., & Characklis, G. W. (2023). Systemic Financial Risk Arising From Residential Flood Losses. *Earth's Future*, *11*(4), 86. https://doi.org/10.1029/2022EF003206

Titley, H. A., Cloke, H. L., Harrigan, S., Pappenberger, F., Prudhomme, C., Robbins, J. C., et al. (2021). Key factors influencing the severity of fluvial flood hazard from tropical cyclones. *Journal of Hydrometeorology*, *22*(7), 1801–1817. https://doi.org/10.1175/JHM-D-20-0250.1

Torres, J. M., Bass, B., Irza, N., Fang, Z., Proft, J., Dawson, C., et al. (2015). Characterizing the hydraulic interactions of hurricane storm surge and rainfall-runoff for the Houston-Galveston region. *Coastal Engineering*, *106*, 7–19. https://doi.org/10.1016/j.coastaleng.2015.09.004

Trigg, M. A., Birch, C. E., Neal, J. C., Bates, P. D., Smith, A., Sampson, C. C., et al. (2016). The credibility challenge for global fluvial flood risk analysis. *Environmental Research Letters*, *11*(9), 094014. https://doi.org/10.1088/1748-9326/11/9/094014

USACE. (2023). National Levee Database. Retrieved November 13, 2023, from https://levees.sec.usace.army.mil/#/

USGS. (2023a). Lidar Base Specification Appendix 2: Hydro-flattening Reference. Retrieved August 1, 2023, from https://www.usgs.gov/ngp-standards-and-specifications/lidar-base-specification-appendix-2-hydro-flattening-reference

USGS. (2023b). USGS National Water Information System (NWIS) Database. Retrieved December 31, 2022, from https://waterdata.usgs.gov/nwis

Volp, N. D., van Prooijen, B. C., & Stelling, G. S. (2013). A finite volume approach for shallow water flow accounting for high-resolution bathymetry and roughness data. *Water Resources Research*, *49*(7), 4126–4135. https://doi.org/10.1002/wrcr.20324

Ward, P. J., Jongman, B., Salamon, P., Simpson, A., Bates, P., De Groeve, T., et al. (2015). Usefulness and limitations of global flood risk models. *Nature Climate Change*, *5*(8), 712–715. https://doi.org/10.1038/nclimate2742

Wing, O. E. J., Bates, P. D., Sampson, C. C., Smith, A. M., Johnson, K. A., & Erickson, T. A. (2017). Validation of a 30 m resolution flood hazard model of the conterminous United States. *Water Resources Research*, *53*(9), 7968–7986. https://doi.org/10.1002/2017WR020917

Wing, O. E. J., Pinter, N., Bates, P. D., & Kousky, C. (2020). New insights into US flood vulnerability revealed from flood insurance big data. *Nature Communications*, *11*(1), 1444. https://doi.org/10.1038/s41467-020-15264-2

Wing, O. E. J., Quinn, N., Bates, P. D., Neal, J. C., Smith, A. M., Sampson, C. C., et al. (2020). Toward Global Stochastic River Flood Modeling. *Water Resources Research*, *56*(8). https://doi.org/10.1029/2020WR027692

Wing, O. E. J., Smith, A. M., Marston, M. L., Porter, J. R., Amodeo, M. F., Sampson, C. C., & Bates, P. D. (2021). Simulating historical flood events at the continental scale: observational validation of a large-scale hydrodynamic model. *Natural Hazards and Earth System Sciences*, *21*(2), 559–575. https://doi.org/10.5194/nhess-21-559-2021

Woodrow, K., Lindsay, J. B., & Berg, A. A. (2016). Evaluating DEM conditioning techniques, elevation source data, and grid resolution for field-scale hydrological parameter extraction. *Journal of Hydrology*, *540*, 1022–1029. https://doi.org/10.1016/j.jhydrol.2016.07.018

Xu, H., Tian, Z., Sun, L., Ye, Q., Ragno, E., Bricker, J., et al. (2022). Compound flood impact of water level and rainfall during tropical cyclone periods in a coastal city: the case of Shanghai. *Natural Hazards and Earth System Sciences*, *22*(7), 2347–2358. https://doi.org/10.5194/nhess-22-2347-2022

Yankovsky, A. E., Torres, R., Torres-Garcia, L. M., & Jeon, K. (2012). Interaction of Tidal and Fluvial Processes in the Transition Zone of the Santee River, SC, USA. *Estuaries and Coasts*, *35*(6), 1500–1509. https://doi.org/10.1007/s12237-012-9535-6

Ye, F., Huang, W., Zhang, Y. J., Moghimi, S., Myers, E., Pe'eri, S., & Yu, H.-C. (2021). A cross-scale study for compound flooding processes during Hurricane Florence. *Natural Hazards and Earth System Sciences*, *21*(6), 1703–1719. https://doi.org/10.5194/nhess-21-1703-2021

Zhang, Y. J., Ye, F., Yu, H., Sun, W., Moghimi, S., Myers, E., et al. (2020). Simulating compound flooding events in a hurricane. *Ocean Dynamics*, *70*(5), 621–640. https://doi.org/10.1007/s10236-020-01351-x